J Physiol 589.12 (2011) pp 2979–2992

The Journal of Physiology

Striatal cellular properties conserved from lampreys to mammals

Jesper Ericsson, Gilad Silberberg, Brita Robertson, Martin A. Wikström and Sten Grillner

Nobel Institute for Neurophysiology, Department of Neuroscience, Stockholm Brain Institute, Karolinska Institutet, SE-171 77 Stockholm, Sweden

Non-technical summary The striatum is a structure in the forebrain that plays an important role in the control of movements. Diseases that affect this region lead to severe movement disorders, such as Parkinson's disease. We show here in the lamprey, the oldest vertebrate group to emerge, that the characteristic cellular properties of neurons in striatum in many respects are similar to those of mammals. Our results show how specific ion channels, including particular potassium channels (Kir) that are open at very negative membrane potentials help shape the way these cells respond to and transmit neuronal signals. These specific features are thus conserved throughout vertebrate evolution, and contribute thereby to our understanding of the mode of operation of striatum, at a cellular level, and how movements are controlled.

Abstract The striatum of the lamprey, the first vertebrate group to appear in evolution, shows striking similarities to that of mammals with respect to histochemical markers, afferent and efferent projections and the effect of dopamine depletion, which leads to hypokinetic motor symptoms. The cellular properties of lamprey striatal neurons were studied here using patch-clamp recordings in acute striatal slices. Sixty-five per cent of recorded neurons were characterised by a prominent inward rectification due to a K^+ conductance of the Kir type. They had a ramping response with a long delay to the first action potential due to activation of a low-voltage-activated A-type K^+ current. Many such inwardly rectifying neurons (IRNs) had a hyperpolarised resting membrane potential and some had spiny dendrites. The remaining 35% of the neurons (non-IRNs) represent a heterogeneous group, including some with characteristics similar to the fast-spiking interneuron of the mammalian striatum. They showed short-lasting, large afterhyperpolarisations (AHPs) and discharged action potentials at high frequency. None of the recorded neurons were spontaneously active but they received GABAergic and glutamatergic synaptic input. The fact that most lamprey striatal neurons display inward rectification indicates that this is a conserved characteristic of striatal neurons throughout vertebrate phylogeny. This is a cellular property of critical importance for the operations of the striatum in mammals.

(Resubmitted 26 March 2011; accepted after revision 12 April 2011; first published online 18 April 2011)
Corresponding author S. Grillner: Nobel Institute for Neurophysiology, Department of Neuroscience, Stockholm Brain Institute, Karolinska Institutet, SE-171 77 Stockholm, Sweden. Email: sten.grillner@ki.se

Abbreviations AHP, afterhyperpolarisation; 4-AP, 4-aminopyridine; DAB, diaminobenzidine; IRN, inwardly rectifying neuron; Kir, inwardly rectifying potassium channels; MPTP, 1-methyl-4-phenyl-1,2,3,6-tetrahydropyridine; MSN, medium spiny neuron; PIR, post-inhibitory rebound.

DOI: 10.1113/jphysiol.2011.209643

Introduction

In the mammalian striatum, 95% of all neurons are GABAergic medium spiny projection neurons (MSNs; cf. Tepper *et al.* 2007). They are characterised by a negative resting potential due to the presence of potassium channels of the inward rectifier type (Kir) that are open at negative potentials, but closed when the membrane potential is brought to more depolarised levels by synaptic excitatory drive. This property of MSNs makes them difficult to activate by the glutamatergic input from cortex and thalamus (Wilson & Kawaguchi, 1996; Tepper *et al.* 2004; Grillner *et al.* 2005). The responsiveness of MSNs is, however, regulated by the degree of dopaminergic modulatory drive (Surmeier *et al.* 2007; Redgrave *et al.* 2008). Without the presence of a dopamine input, mammals become hypokinetic and acquire Parkinsonian symptoms. Conversely, an enhanced level of dopamine leads to hyperkinesias with an unintended initiation of motor programmes.

Kir was recently shown to be a characteristic feature of MSNs in reptiles (Barral *et al.* 2010), which would suggest that Kir is an important property of striatal function in all amniotes (Kawaguchi *et al.* 1989; Farries & Perkel, 2000). Other characteristic features of MSNs are hyperpolarised resting potentials and a ramping response with a long delay to the first action potential due to low-voltage-activated A-type K^+ channels (Kawaguchi *et al.* 1989; Uchimura *et al.* 1989; Nisenbaum & Wilson, 1995).

Cyclostomes (jawless fish like lampreys) represent the first vertebrate group to emerge in evolution. They deviated from the evolutionary line leading up to mammals already 530–560 million years ago, around 200 million years before reptiles emerged (Olsen, 2007). Although a striatum is present in all vertebrates, no information regarding the presence of Kir is available in amphibians, fish or cyclostomes (anamniotes). Recent findings in the lamprey striatum show that it contains spiny GABAergic projection neurons that express dopamine D1 and D2 receptors, tachykinins and enkephalin (Pombal *et al.* 1997*b*, 2001; Auclair *et al.* 2004; Ericsson *et al.* 2010; Robertson *et al.* 2010). Striatum receives input from pallium (cortex in mammals) and thalamus, as well as a dopaminergic, 5-HT and histaminergic input (Brodin *et al.* 1990*a*,*b*; Jimenez *et al.* 1996; Pombal *et al.* 1997*a*). The lamprey striatum thus receives the same type of input and expresses the same molecular markers as in mammals and other amniotes. Dopamine depletion with 1-methyl-4-phenyl-1,2,3,6-tetrahydropyridine (MPTP) renders the lamprey hypokinetic, as in Parkinson's, an effect that can be counteracted by dopamine agonists (Thompson *et al.* 2008). It thus appears that also with regard to function, the role of the basal ganglia is conserved.

In this study we wanted to characterise neurons in the lamprey striatum in terms of their electrophysiological, morphological and synaptic input, and isolate some of the key properties supporting generic striatal function in vertebrates.

Methods

Ethical approval

All experimental procedures conformed to the guidelines of the Stockholm municipal committee for animal experiments.

Slice preparation

Coronal brain slices, 300–500 μm thick, were prepared from 46 lampreys (*Lampetra fluviatilis*), as described earlier (Ericsson *et al.* 2007). Usually only one brain slice per animal containing the striatum, located lateral to the medial telencephalic ventricle (Fig. 1*A* and *B*), in both hemispheres was obtained due to the small size of the striatum. The striatum can be clearly seen as a well-defined band of cell bodies (Fig. 1*A*–*C*). These cells are GABAergic and express substance P and enkephalin, and D1 and D2 receptors (Pombal *et al.* 1997*b*; Robertson *et al.* 2007, 2010). Slices were kept at 4–8°C in artificial cerebrospinal fluid (aCSF) of the following composition (in mM): 125 NaCl, 2.5 KCl, 1 $MgCl_2$, 1.25 NaH_2PO_4, 2 $CaCl_2$, 25 $NaHCO_3$ and 20 glucose. The aCSF was oxygenated continuously with 95% O_2 and 5% CO_2 (pH 7.4) and was also used for perfusion during recordings at the same temperature (Badkontroller V, Luigs & Neumann, Ratingen, Germany).

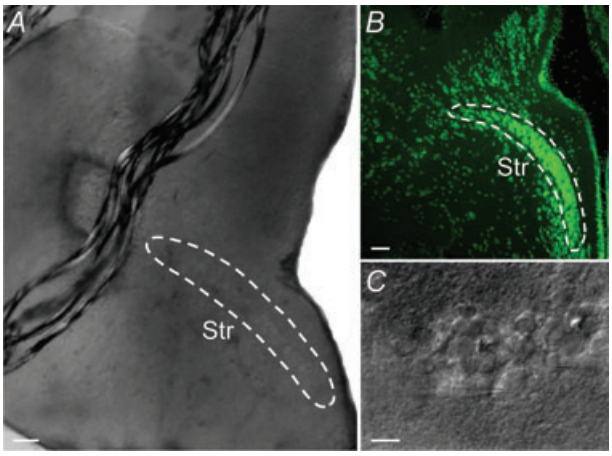

Figure 1. Anatomical location of the striatum (Str)
A, coronal acute brain slice in the recording chamber showing the striatal cell band inside the white lines. *B*, fluorescent Nissl staining of a coronal section displaying the band of striatal cell bodies. *C*, photograph of individual striatal neurons in the recording chamber. Scale bars = 100 μm in *A* and *B*, 15 μm in *C*.

Electrophysiology and morphological reconstruction

Patch-clamp electrodes (7–12 MΩ) were filled with (in mM): 102 KCH_3SO_4, 1.2 $MgCl_2$, 10 Hepes, 1 $CaCl_2$, 10 EGTA, 3.94 Mg-ATP, 0.3 Na-GTP, 5 phosphocreatine sodium salt and 10 glucose (osmolarity 265–275 mosmol l^{-1}) or with an alternative solution with a higher chloride concentration: 105 potassium gluconate, 30 KCl, 10 Hepes, 4 Mg-ATP, 0.3 Na-GTP and 10 phosphocreatine sodium salt (osmolarity 270 mosmol l^{-1}). Patch electrodes were prepared from borosilicate glass microcapillaries (Harvard Apparatus, Edenbridge, UK) using a two-stage puller (PP-830, Narishige, Japan). Whole-cell recordings were performed in current- or voltage-clamp mode using a Multiclamp 700B amplifier (Molecular Devices, Sunnyvale, CA, USA) and digitised at 10–50 kHz by a PC. Bridge balance and pipette capacitance compensation were automatically adjusted on the amplifier and all membrane potential values were corrected for the liquid junction potential. Neurons were visualised (see example in Fig. 1*A* and *C*) with DIC/infrared optics (Zeiss Axioskop 2FS plus, Munich, Germany) and electrodes were advanced using remote micromanipulators (Luigs & Neumann). Data was acquired with the Clampex software and analysed in Clampfit (pCLAMP, Molecular Devices).

Neurons were intracellularly stained by injection of 0.3–0.5% neurobiotin (Vector Laboratories, Burlingame, CA, USA) during recordings. Brain slices were fixed overnight in 4% formalin and 14% picric acid in 0.1 M phosphate buffer (PB) and analysed by either confocal or conventional light microscopy. For confocal imaging (Carl Zeiss LSM 510 Meta, München, Germany), slices were first incubated in streptavidin-Cy2 (1:1000, Jackson Immunoresearch Laboratories, West Grove, PA, USA) in 0.3% Triton X-100 and 1% BSA in 0.1 M PB overnight. The slices were then washed in 0.01 M phosphate buffered saline (PBS) before being dehydrated in alcohol and transferred to methyl salicylate (Merck, NJ, USA) prior to mounting in DPX (Fluka/Sigma-Aldrich, St Louis, MO, USA). Confocal image reconstructions were made and analysed using Zeiss LSM Image Browser and ImageJ software (Rasband WS, National Institutes of Health, Bethesda, MD, USA). Some slices were instead processed with the Vectastain Elite ABC kit (Vector Laboratories). Slices were thoroughly washed in 0.01 M PBS and incubated in 0.6% hydrogen peroxidase in methanol for 20 min, rinsed in PBS and transferred to the ABC solution for 3 h. After rinsing in PBS, slices were incubated in diaminobenzidine (DAB; ImmPACT DAB, Vector Laboratories) for 5 min, then rinsed and dehydrated in alcohol prior to mounting in DPX. Subsequently, neurons were visualised in a light microscope (Olympus BX51, Melville, NY, USA) and photomicrographs were taken using Cell A (Olympus).

Formalin fixed lamprey brain sections, 20 μm thick, were stained with a green fluorescent Nissl stain (1:1000; Molecular Probes Europe BV, Leiden, the Netherlands) for analysis of striatal morphology.

Electrophysiological analysis

Neurons that had stable responses with large over-shooting (reaching above 0 mV) action potentials (mean amplitude ∼54 mV) during step depolarisations in current clamp recordings were considered healthy and were subsequently analysed (see for example Fig. 2*A*). Most recordings were performed in current clamp mode, with injections of hyperpolarising and depolarising current steps to investigate voltage responses. Action potentials were triggered by positive current pulses and the amplitude measured relative to the firing threshold.

The time delay to the first action potential was measured on the first current injection step that elicited an action potential, in a series of increasing steps from a baseline around −75 mV. The input resistance of neurons was calculated by dividing the steady-state voltage response by the applied current injection. A rectification index was defined as the ratio between the input resistance at very hyperpolarised potentials (around −100 to −120 mV) and the input resistance at the resting potential, where no obvious Na^+ conductances had been activated. Thus, large rectification would inversely correspond to a low index since the input resistance at hyperpolarised levels is low while it is significantly higher at more depolarised levels.

To quantify the voltage 'sag' sometimes seen at hyperpolarised potentials, a sag index was calculated. The sag index was defined as the difference of the most hyperpolarised voltage and the steady-state voltage deflection of that pulse (Sag ΔV in Fig. 4*A*) divided by the steady-state deflection. Thus, a large voltage sag correspond to a high sag index, so for example an index of 1 would correspond to an amplitude of the hyperpolarised voltage that was twice as large as the steady-state response.

The average action potential frequency in a spike train was measured between the first and the last action potential during a 1 s suprathreshold current injection. Spontaneous synaptic inputs were recorded using an alternative intracellular solution with 30 mM KCl in the pipette solution to ensure that GABAergic events were detected more easily as depolarising events at the resting potential. These were measured in current clamp mode and analysed by monitoring the frequency of events before and during bath application of drugs.

The following drugs were used and applied directly in the extracellular bath: the K^+ channel blocker 4-aminopyridine (4-AP, 100–500 μM, Sigma-Aldrich, St Louis, MO, USA), Barium chloride (100 μM Sigma-Aldrich), the monovalent cation current I_h antagonist ZD 7288 (50 μM, Tocris Bioscience, Ellisville, MO, USA), the

AMPA receptor antagonist NBQX disodium salt (40 μM, Tocris) and the $GABA_A$ receptor antagonist gabazine (40 μM, Tocris).

Statistics

Results are presented as means ± standard deviation (SD) and statistical comparisons between means were made with Student's two-tailed paired *t* test with GraphPad Prism Software (GraphPad Software, San Diego, CA, USA).

Results

Whole-cell recordings were obtained from 74 neurons that were classified into two main subgroups based on the presence or absence of inward rectification observed by injection of depolarising and hyperpolarising current steps. Pronounced inward rectification is a hallmark of MSNs in amniotes and clearly differentiates these neurons from other striatal interneurons and is therefore of special interest (Kawaguchi *et al.* 1989; Grillner *et al.* 2005; Barral *et al.* 2010). It is identified by lower input resistance at more negative potentials due to the opening of K^+ (Kir) channels (Uchimura *et al.* 1989). An example of an inwardly rectifying neuron is depicted in Fig. 2*A*. The rectification in lamprey striatal neurons was quantified by calculating the ratio between the input resistance at −120 mV and at resting potential (Fig. 2*B* and *C*). Two clusters of neurons with rectification ratios below or above 0.5 were apparent when plotting the rectification ratios (Fig. 2*B*). Forty-eight neurons (65%) had rectification values below 0.5 and displayed clear inward rectification, seen by visual inspection of the voltage responses to stepwise hyperpolarising and depolarising current injections at subthreshold values, and are referred to as inwardly rectifying neurons (IRNs). The population of neurons with rectification values above 0.5 did not show marked inward rectification (Fig. 6) and are

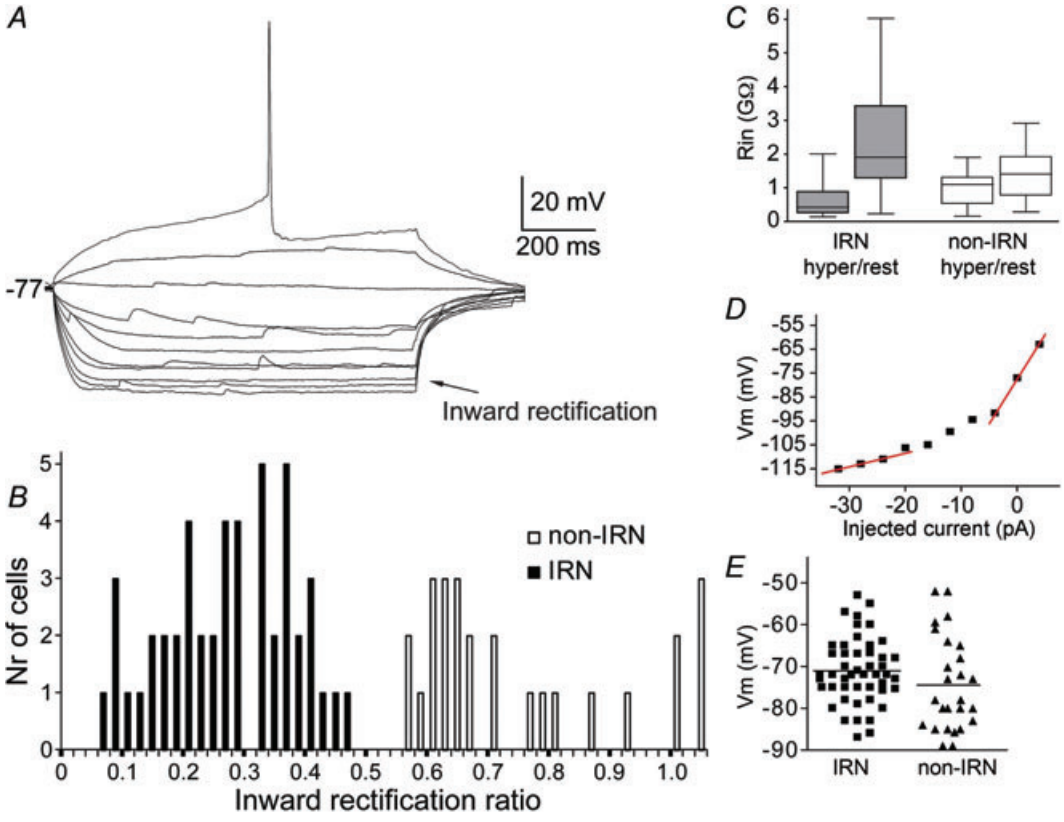

Figure 2. Properties of IRNs and distribution of parameters of both IRNs and non-IRNs
A, voltage responses of an IRN to hyperpolarising and depolarising 1 s current steps of 4 pA per step, elicited from rest at −77 mV. Inward rectification is seen as relatively small voltage responses at hyperpolarised potentials (arrow) with each step and increasingly larger responses at more depolarised levels. The rectification ratio is 0.34. *B*, histogram of the inward rectification ratio for all neurons. Neurons with ratio below 0.5 form a population defined as IRNs and those above 0.5 as non-IRNs. *C*, plot of the input resistance (R_{in}) of IRNs and non-IRNs, measured at a hyperpolarised potential (−120 mV) and at resting membrane potentials. *D*, *I–V* plot of the steady-state voltage deflections to current steps of the neuron displayed in *A*. Note the steeper slope at more depolarised potentials. *E*, distribution of the resting membrane potentials of recorded neurons.

Table 1. Cellular properties of lamprey striatal neurons

	IRNs	non-IRNs
Neurons (*n*)	48	26
Resting potential (mV)	−71.2 ± 7.8	−74.2 ± 11.7
Inward rectification ratio	0.28 ± 0.10	0.75 ± 0.17
Delay to AP (ms)	420 ± 135	345 ± 110
AP amplitude (thr to peak) (mV)	54.4 ± 10.9	55.4 ± 10.2
AP half-width (ms)	3.3 ± 1.6	3.4 ± 1.4
AP threshold (mV)	−46.4 ± 4.4	−46.9 ± 4.1
Amplitude of monophasic AHP (mV)	−22.8 ± 6.3	−18.9 ± 6.8
Neurons with both fAHP and sAHP (*n*)	6	7
Neurons with spike frequency adaptation (*n*)	3	7
Neurons with PIR APs (*n*)	18	4

All values are means ± SD. AP, action potential; AHP, afterhyperpolarization; PIR, post-inhibitory rebound; thr, threshold.

referred to as 'non-IRNs'. We recognise that some neurons classified as non-IRNs here still exhibit a certain degree of inward rectification as indicated by the inward rectification ratio in Fig. 2*B*. No neurons fired action potentials at rest. The basic membrane properties of the two groups are summarised in Table 1.

Inwardly rectifying neurons

Basic electrophysiological properties. IRNs displayed a characteristic voltage response due to inward rectification, hyperpolarised resting membrane potentials and a ramping response to depolarising current injections resulting in a long delay to the first action potential. Figure 2*A* shows the typical appearance of an IRN with an inward rectification ratio of 0.34, with an overall mean ratio for the IRN population of 0.28 ± 0.10, ranging from 0.07 to 0.45 (Fig. 2*B*). Many cells (25%) displayed very strong rectification (ratio ≤0.20). The input resistance was much lower at hyperpolarised membrane potential levels than at rest within the IRN population (Fig. 2*C*). The strongest rectification was normally seen below −90 mV, similar to findings in rodents although not as pronounced (Kawaguchi *et al.* 1989; Jiang & North, 1991; Cepeda *et al.* 2008). The steady state *I–V* curve in Fig. 2*D* shows the characteristic difference in slope between hyperpolarised and more depolarised membrane potential levels, as is evident also from the current steps in Fig. 2*A*. IRNs had a mean resting potential of −71.2 ± 7.8 mV, with 65% of the neurons having values between −70 mV and −87 mV (see Fig. 2*E* for distribution).

Most IRNs (87.5%) displayed a monophasic AHP (Fig. 3*A*). The mean size of the monophasic AHP for IRNs was −22.8 ± 6.3 mV, as measured with reference to the threshold of the action potential, rather than the resting membrane potential. The voltage dependence of the monophasic AHP is illustrated in Fig. 3*A*. The size of the AHP was increased upon depolarisation and was reversed at levels around −75 to −80 mV, indicating that the underlying current was a K^+ current. The time to peak of the AHP was variable (Fig. 3*B*) with a mean of 30.5 ± 19.9 ms for the neurons with monophasic AHPs. Six IRNs (12.5%) displayed a biphasic AHP with the time to the second maximum ranging from 41 ms to 170 ms, and with a mean of 89.8 ± 45.7 ms. The mean amplitude of the slow AHP (sAHP) was −15.8 ± 5.0 mV. The time to the peak of the fast AHP (fAHP) component was 9.1 ± 4.0 ms. Half of these neurons showed a marked spike frequency adaptation with comparable properties to the neuron displayed in Fig. 6*G*.

Seventy per cent of IRNs showed reliable and regular spiking with a limited spike frequency adaptation during sustained current injections (Fig. 3*C* and *D*), while the other 30% of neurons had some broadening of action potentials, firing failure at depolarised levels and sometimes irregular firing patterns. Action potentials had a threshold of −46.4 ± 4.4 mV, a half-width of 3.3 ± 1.6 ms and amplitude of 54.4 ± 10.9 mV (see Table 1). Fifty per cent of IRNs could discharge at frequencies of 15 Hz or above for a sustained period and a few (6%) up to at least 50 Hz. Most neurons appeared to saturate at their maximum firing frequencies, while the remainder showed action potential inactivation at further depolarisation.

Some of the IRNs showed a time- and voltage-dependent sag in their response to hyperpolarising current steps (Fig. 4*D*), contributing with a time-dependent component of the inward rectification. The sag was estimated by a sag index (see Methods), as exemplified by the cell in Fig. 4*D* with a sag index of 0.31. Only a minority (33%) of the IRNs (Fig. 4*F*), however, had a sag index 0.2 or above, a value not reached by any of the non-IRNs. The sag was most pronounced at hyperpolarised potentials and in many of these neurons it was not visible at voltages more depolarised than

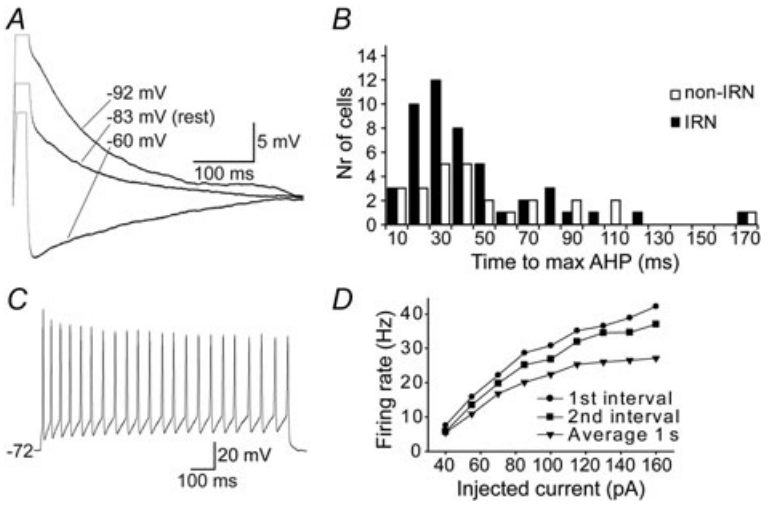

Figure 3. Afterhyperpolarisation (AHP) and firing properties of IRNs
A, the AHP of an IRN following the action potential elicited by a 5 ms positive current pulse. The AHP is shown at three different baseline potentials (−60, −83 and −92 mV), achieved by continuous current injections, to reveal the voltage dependence of the AHP. The AHP is reversed between −60 mV and −83 mV. *B*, frequency histogram of the time to maximum AHP for IRNs (black) and non-IRNs (white). *C*, response to suprathreshold current injections, showing the firing properties of the neuron in *A*. *D*, plot of firing rate as a function of the injected current during a 1 s current pulse in the neuron in *C*. The round markers indicates the instantaneous frequency of the first interval in the elicited train of action potentials and the squares the second interval. The triangles show the average firing frequency over the entire train of action potentials.

at −85 mV. At the termination of the hyperpolarising steps that were elicited from rest, a post-inhibitory rebound (PIR) depolarisation with spiking occurred (Fig. 4*D*) in 60% of these neurons with a sag index of 0.2 or larger. The larger the hyperpolarising steps, the greater the PIR depolarisation and the number of action potentials generated (up to 8 action potentials). PIR spikes could, however, also be elicited in a subset of IRNs without a sag when the hyperpolarising pulses were injected from depolarised baselines around −60 mV but not at the more hyperpolarised resting state.

Pharmacological analysis of inward rectification in IRNs. The Kir channels have been investigated in different species and cell types, including rat dorsal and ventral striatal cells, and they are known to be blocked by extracellular barium chloride at 100 μM (Standen & Stanfield, 1978; Uchimura *et al.* 1989; Nisenbaum & Wilson, 1995). Through bath

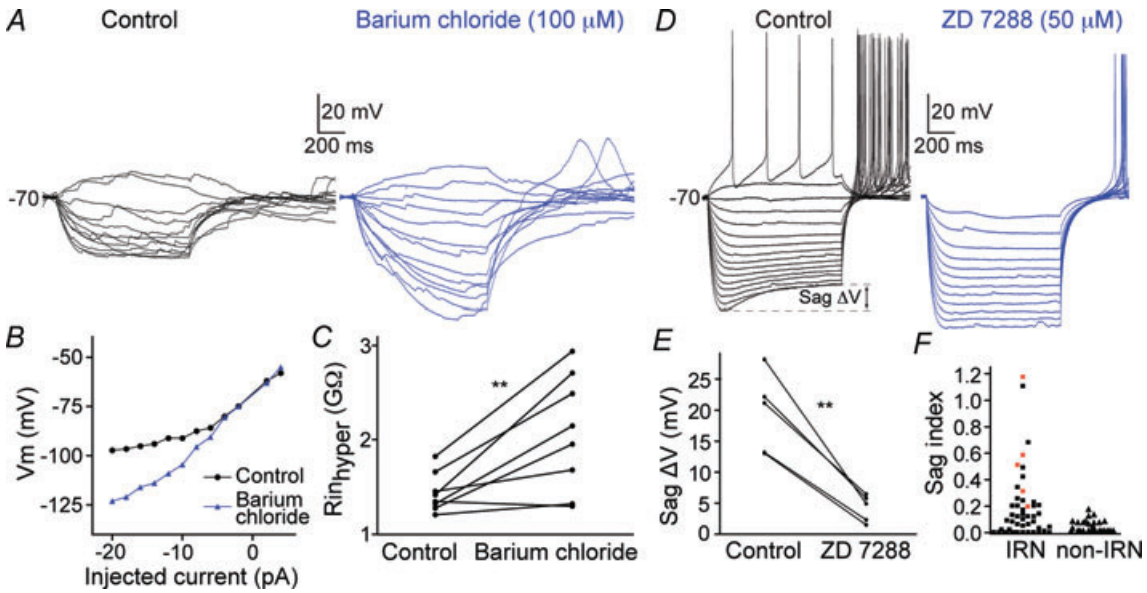

Figure 4. Pharmacological analyses of Kir and I_h in IRNs
A, voltage responses of an IRN before (left) and during bath application of barium chloride (right) that blocks Kir-channels. *B*, *I–V* plot of the cell in *A*, that shifts from being upwardly concave (control) to a close to straight line (barium chloride). *C*, the input resistance at hyperpolarised potentials is increased during Ba^{2+} application. *D*, the left voltage traces shows an IRN that also displays an I_h-induced sag (see Sag ΔV) with a sag index of 0.31, followed by a post-inhibitory rebound with action potentials at the end of the hyperpolarising current steps. Under control conditions (left) the I_h sag is seen clearly at hyperpolarised levels while bath application of the I_h antagonist ZD 7288 almost completely removes the sag (right). *E*, the sag is reduced after application of ZD 7288 (50 μM, $n = 5$). *F*, plot of the sag index for each IRN and non-IRN. The paler squares indicate the neurons in which ZD 7288 was applied.

application of barium chloride at this concentration, we show that the inward rectification is significantly reduced at subthreshold levels (Fig. 4*A*–*C*, $n = 8$). Figure 4*A* shows an IRN before and during Ba^{2+} application, with increased voltage deflections between each current stimulation and prolonged time-constants. The *I*–*V* relationship (Fig. 4*B*) changes from an upwardly concave curve to an almost straight line, reflecting a near constant input resistance below rest after the blockade with Ba^{2+}. The effect of Ba^{2+} was quantified by comparing the input resistance at hyperpolarised potentials (around −110 mV) before and during barium and it increased significantly from 1.44 ± 0.2 GΩ to 2.06 ± 0.6 GΩ ($P < 0.01$, $n = 8$; Fig. 4*C*). The degree of rectification was associated with the change in input resistance, so that neurons with less rectification showed less change and the one neuron in Fig. 4*C* that did not increase its input resistance was also clearly defined as a non-IRN based on its inward rectification ratio (0.93). The application of Ba^{2+} was also accompanied by a depolarisation of neurons by 5–10 mV.

The effect of Ba^{2+} on the inward rectification in striatal neurons suggest that it is due to Kir-channels, and thus also due to a K^+ conductance.

Pharmacological analyses of I_h and A-type K^+ current contribution to IRNs. One-third of the IRNs had a voltage-dependent sag (Fig. 4*D* and *F*) that was examined by bath application of 50 μM ZD 7288, an antagonist of the monovalent cation current I_h known to cause a voltage sag in other neurons (Harris & Constanti, 1995). Following ZD 7288 application, the sag decreased markedly from 19.5 ± 6.4 mV to 4.3 ± 2.2 mV ($P < 0.01$, $n = 5$; Fig. 4*D* and *E*). Figure 4*D* also shows that the inward rectification was reduced but maintained at a lower level after application of ZD 7288. In one neuron, Ba^{2+} was added 10 min following application of ZD 7288, effectively removing all inward rectification (data not shown). ZD 7288 also affected the PIR depolarisation and the accompanying action potentials. The time to the first rebound action potential increased from 104 ± 24 ms to 235 ± 48 ms ($P < 0.05$, $n = 4$), and the number of rebound action potentials was reduced by 1–4 action potentials (Fig. 4*D*). These data clearly indicate that the sag is mediated by activation of an I_h current and partly also the accompanying PIR.

The characteristic ramping response and long delay to the first action potential in rat MSNs is mainly due to activation of a low-voltage-activated K^+ current, I_A, activated at subthreshold membrane potentials and that inactivates after hundreds of milliseconds (Surmeier *et al.* 1991; Nisenbaum & Wilson, 1995; Shen *et al.* 2004). In lamprey, as well as mammals, this A-type K^+ current is selectively depressed at low concentrations of 4-AP (100 μM), while high concentrations also reduce the high-voltage-activated A-type K^+ current (Rogawski *et al.* 1985; Surmeier *et al.* 1991; Nisenbaum & Wilson, 1995; Hess & El Manira, 2001). During investigation of the low-voltage-activated A-type K^+ channels, neurons were held at very hyperpolarised levels to ensure that these channels were not voltage inactivated before the depolarising steps were given (Fig. 5*A*). 4-AP reduced the time delay to the first action potential (Fig. 5*A* and *B*) at a concentration of both 100 μM ($P < 0.05$, control: 518 ± 93 ms; 100 μM: 211 ± 8 ms, $n = 3$) and 500 μM ($P < 0.01$, control: 522 ± 84 ms; 500 μM: 234 ± 47 ms, $n = 5$). Similar results were obtained through voltage inactivation of the A-type K^+ current by membrane depolarisation before current injections (Fig. 5*C* and *D*). The delay to the first action potential was reduced from 460 ± 92 ms to 151 ± 99 ms by changing the baseline membrane potential from −90 mV to −60 mV ($P < 0.01$, $n = 5$). It should be noted, however, that the long delays to first spike are present at rest in neurons (Fig. 2*A* and Table 1). These results suggest that an A-type K^+ current

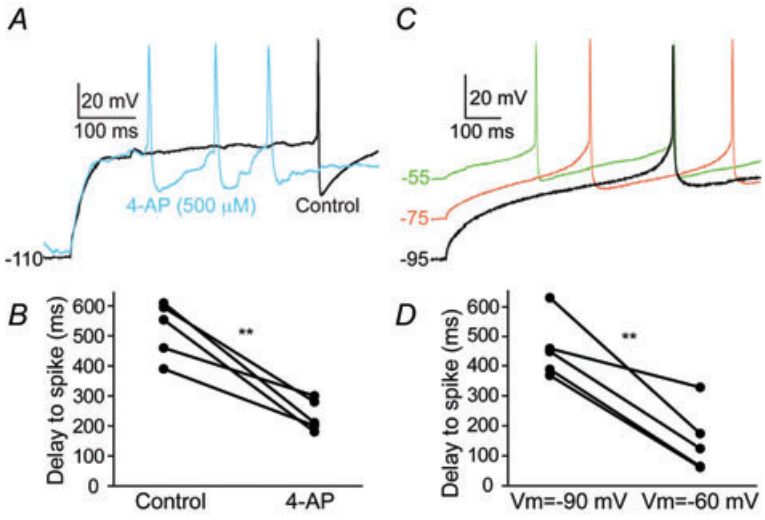

Figure 5. Pharmacological analyses of the A-type K^+ current contribution to IRNs
A, voltage response to the first depolarising current step that elicits an action potential (black line, control) displaying the long delay to first action potential. During bath application of the I_A antagonist 4-AP at 100 and 500 μM action potentials are evoked after a much shorter delay. Data only shown for 500 μM. *B*, the time delay to the first action potential is reduced by several hundred milliseconds by 4-AP (500 μM, $n = 5$). *C*, the ramping response to first spike is also reduced by eliciting action potentials from different baseline potentials. The more depolarised baseline potential (from lower to middle to upper traces), the shorter the time-delay to first action potential. *D*, at −60 mV, the time delay to first action potential is significantly shorter than at −90 mV ($n = 5$).

contributes to the ramping response with a long delay to the first spike, upon a depolarisation from a hyperpolarised level.

Synaptic input to IRNs. Lamprey striatal neurons receive glutamatergic spontaneous synaptic input (Ericsson *et al.* 2007). We show that striatal neurons also receive a continuous GABAergic input (Fig. 6*A* and *B*). Application of the $GABA_A$ receptor blocker gabazine (40 μM) strongly reduced the spontaneous input ($P < 0.01$, control: 5.48 ± 1.61 Hz; gabazine: 2.48 ± 1.36 Hz, $n = 5$). Further application of NBQX (40 μM) blocked almost all of the remaining synaptic input ($P < 0.01$, gabazine: 2.48 ± 1.36 Hz; NBQX+gabazine: 0.10 ± 0.17 Hz, $n = 5$). To facilitate the detection of GABAergic input at the resting membrane potential, these experiments were performed with an intracellular solution containing 30 mM chloride, thus shifting the reversal potential for $GABA_A$ responses to a predicted value around −35 mV.

Non-inwardly rectifying neurons

Basic electrophysiological properties. Non-IRNs represent a somewhat heterogeneous group ($n = 26$) and are defined as having a rectification ratio larger than 0.5 (0.75 ± 0.17, ranging from 0.56 to 1.05, see Fig. 2*B*), and *I–V* traces with a close to linear relationship (Fig. 7*A* and *B*). The mean resting membrane potential was −74.2 ± 11.7 mV (Table 1), and 69% of the neurons had resting potentials below −70 mV (Fig. 2*E*). Most neurons demonstrated long delays to the first action potential (345 ± 110 ms) with amplitudes of 55.4 ± 10.2 mV (Table 1). The action potential threshold was −46.9 ± 4.1 mV and the half-width 3.4 ± 1.4 ms. When the non-IRNs are taken as a group there are, except for the rectification ratio and the lack of I_h (Fig. 4*F*), no prominent differences in cellular properties compared to IRNs (see Table 1).

One subgroup of non-IRNs displayed a fast monophasic AHP following the action potential (69%; Fig. 7*C*), while the other exhibited a biphasic AHP (Fig. 7*F*). The average time to peak of the monophasic AHP (Fig. 7*C*) was 29.4 ± 16.4 ms, and the amplitude −18.9 ± 6.8 mV, as estimated from the threshold of the action potential. The monophasic AHP reversed at the same membrane potential level as in IRNs, i.e. around −75 to −80 mV (Fig. 7*C*). Seventy-three per cent of non-IRNs with monophasic AHPs showed regular spiking with action potential frequencies ranging from 15 to 40 Hz with limited spike frequency adaptation. Three of the neurons with a monophasic AHP appeared to represent a separate subcategory of non-IRNs. They displayed significantly shorter times to peak AHP (8.3 ± 3.2 ms), narrow action potentials (1.75 ± 0.06 ms, cf. Table 1) and high frequency spiking up to 60 Hz with very modest spike frequency adaptation, as measured over 1 s, and over 80 Hz for the first interval (example in Fig. 7*D* and *E*). In addition, two of these neurons had very low input resistance, both at hyperpolarised potentials (340 ± 70 MΩ) and at rest (490 ± 7 MΩ).

The non-IRNs that displayed biphasic AHPs (27%, Fig. 7*F*) had a time to the second peak of 90.4 ± 42.1 ms (Fig. 3*B*) with an amplitude of −17.4 ± 3.6 mV. The time to the fAHP component was 10.3 ± 4.3 ms. The majority of these neurons showed a marked spike frequency adaptation (Fig. 7*G* and *H*), and a frequency range from 10–30 Hz.

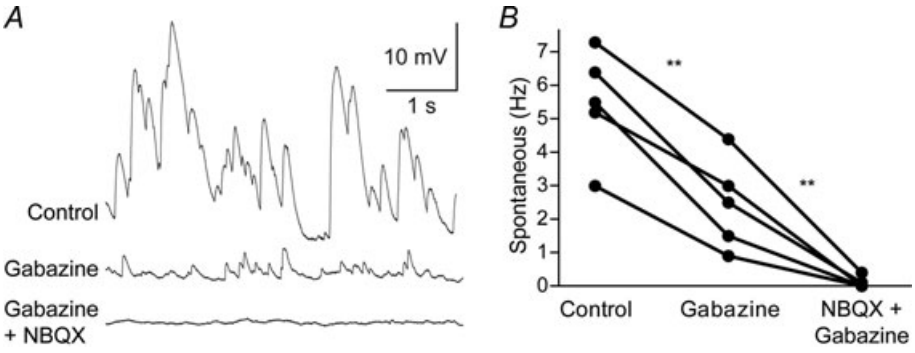

Figure 6. Spontaneous synaptic input to IRNs
A, current clamp recordings of spontaneous synaptic input at −85 mV. The upper trace shows synaptic input during control conditions, the second during bath application of the $GABA_A$ receptor antagonist gabazine (40 μM) and the third during bath application of gabazine and the AMPA receptor antagonist NBQX (40 μM) simultaneously. *B*, gabazine significantly reduces the spontaneous synaptic input and additional application of NBQX almost completely blocks all spontaneous synaptic input. All spontaneous synaptic input recordings were performed with intracellular solutions containing moderate concentrations of Cl^- so that GABAergic input is reversed at more depolarised potentials (theoretically around −35 mV).

Morphology and topography

Morphological properties. A total of 12 IRNs and 12 non-IRNs were labelled. There was no apparent difference in somatic characteristics of IRNs and non-IRNs as both had fusiform or spherical shapes. The somata diameters ranged from 8 to 15 μm and the cell bodies were located within the striatal cell band or just lateral to the cell band where substance P expressing striatal neurons are located (Fig. 8*A*–*E*; Nozaki & Gorbman, 1986).

Most labelled neurons (8 IRNs and 8 non-IRNs) had two major processes that extended in opposite directions diagonally from the soma (see for example Fig. 8*B* and *C*), while the rest had either three to five processes or only one process. Each neuron generally had one thinner, uniform process and one thicker process with a broad base of 2–3 μm that gradually became thinner and progressed with a thickness of 0.5–1 μm. The thin processes are putative axons that originated either directly from the soma or by branching off in a right angle from the base of a proximal dendrite. These processes were difficult to follow due to their thin diameters. Most of our reconstructions within the coronal plane probably represent dendrites, based on their non-uniform thickness and oblique branching. Figure 8*F* shows original confocal reconstructions, including the two non-IRNs in Fig. 8*C*, demonstrating the moderate branching exhibited by some cells. Many processes, especially those in the area between the striatum and the ventricle, had varicosities about 2 μm apart from each other.

Neurons in the lamprey striatum have been described to have dendritic spines (Pombal *et al.* 1997*b*). Figure 8*G* shows an overview of a spiny IRN located in the caudal striatum, visualised with DAB staining. The spiny dendritic process is shown in close-up in Fig. 8*H*. Another

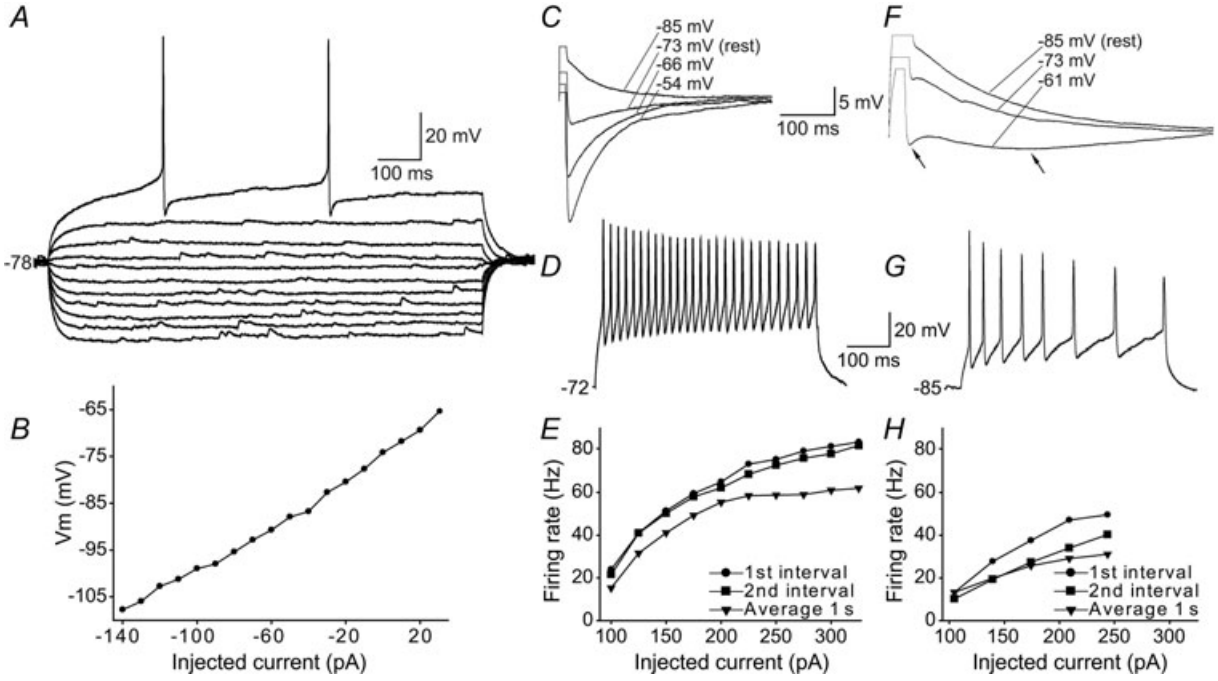

Figure 7. Properties of non-IRNs
A, voltage responses of a non-IRN to hyperpolarising and depolarising 1 s current steps of 10 pA per step, elicited from rest at −78 mV. The displayed neuron lacks inward rectification with a rectification ratio of 0.78 and also lacks any obvious sag. *B*, *I–V* plot of the steady-state voltage deflections to current steps of the neuron displayed in *A* showing close to a linear relationship. *C*, monophasic afterhyperpolarisation (AHP) response after an action potential elicited by a 5 ms positive current injection. The voltage dependence of the AHP is shown by recordings at four different baseline potentials. The reversal of the AHP takes place between −73 and −85 mV in this neuron. Scale bar for both panels *C* and *F*. *D*, response to suprathreshold current injections in another non-IRN with large, fast AHP showing its firing properties. Same scale bar for panels *D* and *G*. *E*, plot of firing rate as a function of the injected current during a 1 s current pulse of the neuron in *D*. The round markers shows the instantaneous frequency of the first interval in the train of action potentials, the squares the second interval and the triangles the average firing frequency over the entire train of action potentials. This cell also had low input resistance ($R_{in,hyper}$ = 290 MΩ, $R_{in,rest}$ = 380 MΩ) compared to lamprey striatal neurons in general (compare to Fig. 3*A*). *F*, voltage recording of another non-IRN showing a biphasic AHP (arrows) response after the action potential, shown at three different baseline potentials. *G*, response to suprathreshold current injections in a neuron with biphasic AHP showing spike frequency adaptation. *H*, plot of firing rate as a function of the injected current of the neuron above.

spiny dendrite, visualised by confocal microscopy, is displayed in Fig. 8*I*. Spines appeared as thin, short stubs extending from the dendrite or as bulbs located directly on the dendritic shaft. All spiny dendrites were IRNs and they were always distal dendrites but not in perisomatic domains. We could not confirm that spines were present in all IRNs, even when well stained. This may possibly relate to the orientation of the distal dendrites in the striatal slices.

Projections of IRNs and non-IRNs. IRNs located in the rostral striatum had relatively short projections in the coronal plane (Fig. 8*A* and *B*). Instead, most of these processes turned in a perpendicular direction after 50–150 μm and continued in the rostrocaudal direction ($n = 6/7$) towards the pallidal regions of the lamprey (Ericsson *et al.* 2010). However, IRNs located more caudally (Fig. 8*D*) sent longer processes (up to 250 μm) within the same coronal plane and with more branching

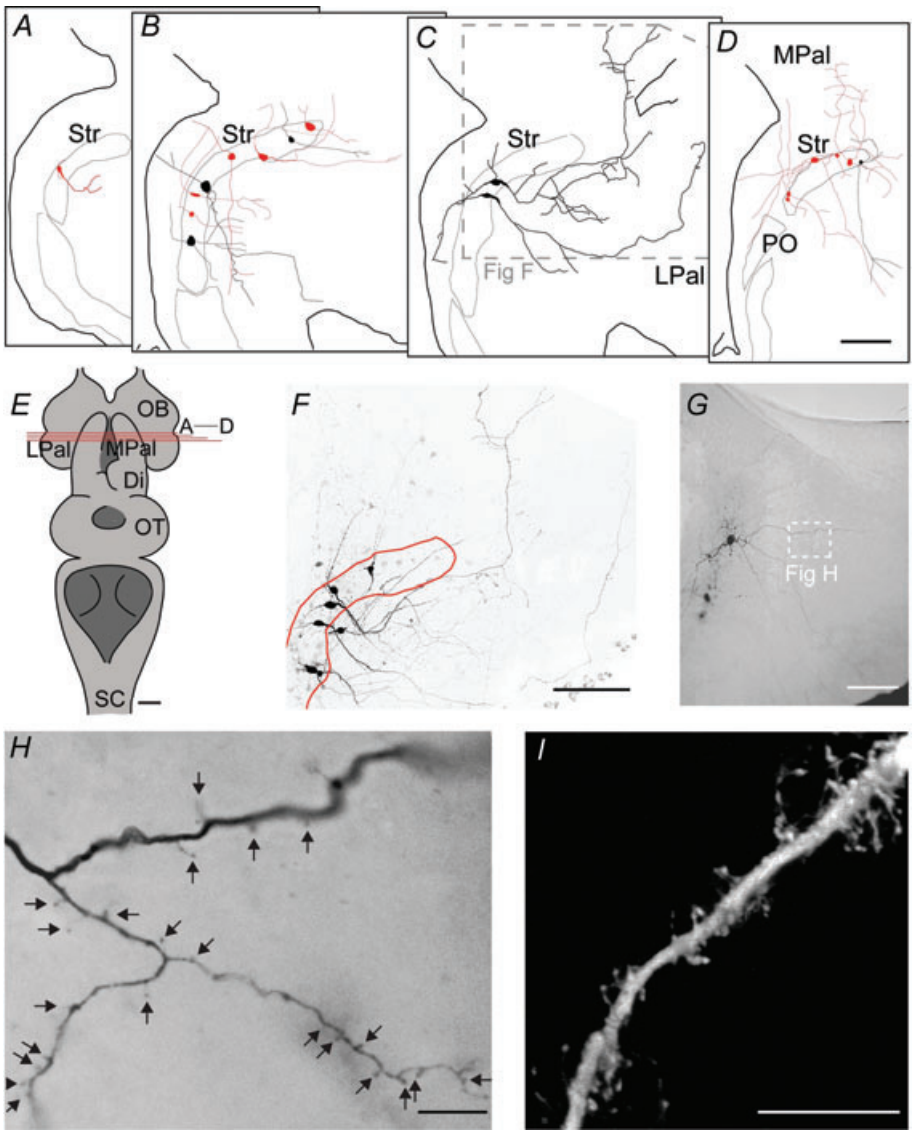

Figure 8. Morphology and topography of striatal neurons
A–D, schematic representations of IRNs (pale) and non-IRNs (black), in sections from rostral to caudal according to *E*. *E*, overview of the lamprey brain, including the level of coronal sectioning shown in *A–D*. *F*, confocal image showing the morphological properties of the two non-IRNs shown in *C*, among 4 other labelled but unrecorded neurons. See inset in *C* for the location in the coronal section. *G*, overview of a spiny IRN by light microscopy of a DAB-stained slice. *H*, close-up of spiny dendrites in the IRN shown in *G*, according to white inset. *I*, confocal image of another spiny dendrite labelled in the striatum. Scale bars = 100 μm in *A–D*, *F* and *G*; 1 mm in *E*; 10 μm in *H* and *I*. Abbreviations are as follows: Di, diencephalon; LPal, lateral pallium; MPal, medial pallium; OB, olfactory bulb; PO, nucleus preopticus; OT, optic tectum; Str, striatum.

and two of these IRNs had processes that also projected rostrocaudally. IRNs extended processes towards both the medial telencephalic ventricle and the medial and lateral pallium (Fig. 8*A–D*) within the coronal plane.

The processes of non-IRNs were mainly distributed within the coronal plane and only one neuron had a clear rostrocaudal projection. Many processes were long (300–700 μm) and in nine neurons they approached or reached into the lateral and ventrolateral pallium.

Discussion

As summarised in the introduction, the lamprey striatum shows many similarities to that of mammals with regard to organisation of input structures and histochemical markers, and a dopamine denervation results in similar types of behavioural effects (Grillner *et al.* 2008; Ménard & Grillner, 2008; Thompson *et al.* 2008). The IRN group forms a distinct cluster with Kir channels and an inward rectification ratio ranging from 0.07 to 0.45 (see Fig. 2*B*). The remaining group, referred to here as non-IRNs, represents a more heterogeneous group.

Comparison of IRNs to neurons of other vertebrates

IRNs share many of the intrinsic properties of mammalian MSNs, i.e. a fast inward rectification due to Kir-channels, hyperpolarised resting membrane potentials and a long delay to the first action potential due to activation of the low-voltage-activated A-type K^+ current (Rogawski *et al.* 1985; Kawaguchi *et al.* 1989; Jiang & North, 1991; Nisenbaum & Wilson, 1995; Shen *et al.* 2007). The majority of lamprey IRNs (65%) exhibit inward rectification due only to Kir. These IRNs may serve a similar function as in mammals, where it contributes to maintain MSNs at hyperpolarised potentials until Kir-channels close upon strong excitatory input (Wilson & Kawaguchi, 1996; Stern *et al.* 1998; Grillner *et al.* 2005). Interestingly, however, around one-third of the IRNs also exhibits a large I_h-induced sag that increases the conductance at hyperpolarised potentials further and amplifies their inward rectification ratio. This subpopulation of IRNs clearly differs from rodent MSNs. Hyperpolarising current steps often triggered post-inhibitory rebound action potentials in this group of IRNs (see Fig. 4*A*). Potentially, a synchronised barrage of inhibitory activity limited in duration may elicit PIR spikes and thereby output from the striatum.

We show that striatal neurons receive both GABAergic and glutamatergic input, and it seems likely that the former is provided by local GABAergic microcircuits since the striatum contains almost exclusively GABAergic neurons (Robertson *et al.* 2007). The glutamatergic input presumably originates from the thalamostriatal or the lateral and medial palliostriatal fibres (Pombal *et al.* 1997*a*; Northcutt & Wicht, 1997). In experiments where the synaptic input was blocked, the resting potential did not change markedly, indicating that it was not significantly influenced by the synaptic input. Once depolarised, the input resistance of IRNs was shown to increase to high values with a mean of 2400 MΩ, as compared to rodent MSNs with maximum input resistances around 600 MΩ depending on the preparation (Kawaguchi, 1993; Tepper *et al.* 2004; Cepeda *et al.* 2008). This difference may be related to the small size of lamprey neurons, but also to the distribution and density of ion channels. Inward rectification in rodents appears more pronounced than in lamprey, possibly due to a higher expression of Kir channels. In rodents, MSNs represent roughly 95% of the striatal neurons (Tepper *et al.* 2004) whereas only 65% of lamprey neurons are classified as IRNs. The population of IRNs, as defined here, may possibly be larger, as a fraction of non-IRNs have a ratio close to the dividing ratio of 0.5.

Striatal neurons are known to project to an area close to eminentia thalami, containing GABAergic projection neurons that target the mesencephalic and dienchephalic locomotor regions (MLR and DLR), as well as tectum (Ménard *et al.* 2007; Ménard & Grillner, 2008; Robertson *et al.* 2007, 2009; Stephenson-Jones *et al.* 2010). This area is suggested to be homologous to that of the mammalian globus pallidus. Recent findings also show striatal projections to an area in the caudolateral tegmentum containing GABAergic neurons projecting to tectum (Robertson *et al.* 2009). New recordings from retrogradely labelled striatal projection neurons suggest that different subsets of IRNs project to the different output regions of the basal ganglia in lamprey (Ericsson *et al.* 2010), thus corresponding to striatal projections in other vertebrates, and show that IRNs represent the striatal output neurons.

Comparison of non-IRNs to neurons of other vertebrates

In the mammalian striatum, only interneurons lack inward rectification (Tepper & Bolam, 2004). A subgroup of non-IRNs had properties similar to the mammalian parvalbumin-expressing fast spiking interneurons, characterised by fast-spiking frequencies, very low spike frequency adaptation, low input resistance, narrow action potentials and short delays to AHPs (Kawaguchi, 1993; Tepper & Bolam, 2004).

Another subgroup was distinguished by their biphasic AHPs and marked spike frequency adaptation. The fast component of the AHP appears to be fairly similar in all lamprey striatal neurons and reversed around −75 to −80 mV. The main current mediating this AHP is likely to be the high-threshold transient A-type K^+

current, which has been investigated in detail in the lamprey spinal cord (Hess & El Manira, 2001; Cangiano *et al.* 2002). The second, slower component seen in some neurons shows similar properties to the slow AHP in lamprey spinal neurons, due primarily to apamin-sensitive calcium-dependent K^+ channels (Cangiano *et al.* 2002) with a residual 20% mediated by a Slack-like subtype of sodium-dependent K^+ channel (Wallén *et al.* 2007).

The morphological data of non-IRNs showed that many of their dendritic processes are within the coronal plane where their cell bodies are located. However, we assume that non-IRNs and especially those resembling the fast-spiking type neurons represent interneurons. Few afferents to the striatum actually innervate the cell layer (Pombal *et al.* 1997*b*) and rather target the periventricular neuropil or the area between the striatal cell layer and the lateral pallium. It thus seems likely that the dendrites of putative interneurons would not respect the boundaries of the cell layer. Although the presumed axons of these cells were too thin to be traced in order to confirm that they only contact other striatal neurons, the results discussed above (e.g. Ericsson *et al.* 2010) with all output neurons identified as IRNs, further strengthen the possibility that they are interneurons.

In the lamprey striatum there is a pronounced acetylcholinesterase activity and cells have been found to express choline acetyltransferase immunoreactivity (Pombal *et al.* 1997*b*, 2001), suggesting the presence of cholinergic neurons. In rodents, large aspiny cholinergic interneurons represent around 1% of the striatal cell population (Rymar *et al.* 2004). In the present sample of cells ($n = 74$), no neurons could clearly be identified as cholinergic cells.

Concluding remarks

Our data further strengthen previous findings suggesting that the basic properties of the striatal neurons had already been developed early in vertebrate evolution, before the lamprey diverged from the main vertebrate line around 560 million years ago. Lamprey striatal neurons express some of the hallmarks of mammalian striatal neurons, including inward rectification due to Kir channels. About one-third of these neurons also display I_h-mediated voltage sags, which would ascertain that after an inhibitory hyperpolarisation there will be an I_h depolarisation that is often accompanied by PIR spikes. These characteristics may be unique to non-mammalian species. This study is the first detailed electrophysiological study of the striatal cell properties in anamniotes and indicates that the principal neuronal type and the fast-spiking interneuron were present some 250–300 million years before the anamniote–amniote transition. Thus, the basic design of the striatum and the basal ganglia circuitry implied in decision-making and action selection of motor behaviour are present even in the less evolved lamprey, supporting a limited behavioural repertoire.

References

Auclair F, Lund J & Dubuc R (2004). Immunohistochemical distribution of tachykinins in the CNS of the lamprey Petromyzon marinus. *J Comp Neurol* **479**, 328–346.

Barral J, Galarraga E, Tapia D, Flores-Barrera E, Reyes A & Bargas J (2010). Dopaminergic modulation of spiny neurons in the turtle striatum. *Cell Mol Neurobiol* **30**, 743–750.

Brodin L, Hokfelt T, Grillner S & Panula P (1990*a*). Distribution of histaminergic neurons in the brain of the lamprey *Lampetra fluviatilis* as revealed by histamine-immunohistochemistry. *J Comp Neurol* **292**, 435–442.

Brodin L, Theordorsson E, Christenson J, Cullheim S, Hökfelt T, Brown J, Buchan A, Panula P, Verhofstad A & Goldstein M (1990*b*). Neurotensin-like peptides in the CNS of lampreys: chromatographic characterization and immunohisto chemical localization with reference to aminergic markers. *Eur J Neurosci* **2**, 1095–1109.

Cangiano L, Wallén P & Grillner S (2002). Role of apamin-sensitive K_{Ca} channels for reticulospinal synaptic transmission to motoneuron and for the afterhyperpolarization. *J Neurophysiol* **88**, 289–299.

Cepeda C, André V, Yamazaki I, Wu N, Kleiman-Weiner M & Levine M (2008). Differential electrophysiological properties of dopamine D1 and D2 receptor-containing striatal medium-sized spiny neurons. *Eur J Neurosci* **27**, 671–682.

Ericsson J, Robertson B & Wikstrom MA (2007). A lamprey striatal brain slice preparation for patch-clamp recordings. *J Neurosci Methods* **165**, 251–256.

Ericsson J, Stephenson-Jones MR, Samuelsson E, Robertson B, Hill R, Hellgren J & Grillner S (2010). The lamprey provides a vertebrate blueprint of the mammalian basal ganglia. Meeting abstract, 142.8, Federation of European Neuroscience Societies Forum.

Farries MA & Perkel DJ (2000). Electrophysiological properties of avian basal ganglia neurons recorded in vitro. *J Neurophysiol* **84**, 2502–2513.

Grillner S, Hellgren J, Menard A, Saitoh K & Wikstrom MA (2005). Mechanisms for selection of basic motor programs – roles for the striatum and pallidum. *Trends Neurosci* **28**, 364–370.

Grillner S, Wallen P, Saitoh K, Kozlov A & Robertson B (2008). Neural bases of goal-directed locomotion in vertebrates – an overview. *Brain Res Rev* **57**, 2–12.

Harris NC & Constanti A (1995). Mechanism of block by ZD 7288 of the hyperpolarization-activated inward rectifying current in guinea pig substantia nigra neurons in vitro. *J Neurophysiol* **74**, 2366–2378.

Hess D & El Manira A (2001). Characterization of a high-voltage-activated IA current with a role in spike timing and locomotor pattern generation. *Proc Natl Acad Sci U S A* **98**, 5276–5281.

Jiang ZG & North RA (1991). Membrane properties and synaptic responses of rat striatal neurones *in vitro*. *J Physiol* **443**, 533–553.

Jimenez AJ, Mancera JM, Pombal MA, Perez-Figares JM & Fernandez-Llebrez P (1996). Distribution of galanin-like immunoreactive elements in the brain of the adult lamprey *Lampetra fluviatilis*. *J Comp Neurol* **368**, 185–197.

Kawaguchi Y (1993). Physiological, morphological, and histochemical characterization of three classes of interneurons in rat neostriatum. *J Neurosci* **13**, 4908–4923.

Kawaguchi Y, Wilson CJ & Emson PC (1989). Intracellular recording of identified neostriatal patch and matrix spiny cells in a slice preparation preserving cortical inputs. *J Neurophysiol* **62**, 1052–1068.

Ménard A & Grillner S (2008). Diencephalic locomotor region in the lamprey – afferents and efferent control. *J Neurophysiol* **100**, 1343–1353.

Ménard A, Auclair F, Bourcier-Lucas C, Grillner S & Dubuc R (2007). Descending GABAergic projections to the mesencephalic locomotor region in the lamprey *Petromyzon marinus*. *J Comp Neurol* **501**, 260–273.

Nisenbaum ES & Wilson CJ (1995). Potassium currents responsible for inward and outward rectification in rat neostriatal spiny projection neurons. *J Neurosci* **15**, 4449–4463.

Northcutt RG & Wicht H (1997). Afferent and efferent connections of the lateral and medial pallia of the silver lamprey. *Brain Behav Evol* **49**, 1–19.

Nozaki M & Gorbman A (1986). Occurrence and distribution of substance P-related immunoreactivity in the brain of adult lampreys, *Petromyzon marinus* and *Entosphenus tridentatus*. *Gen Comp Endocrinol* **62**, 217–229.

Olsen BD (2007). Understanding biology through evolution, 3rd edn, Vol. 25, p. 149.

Pombal MA, El Manira A & Grillner S (1997*a*). Afferents of the lamprey striatum with special reference to the dopaminergic system: a combined tracing and immunohistochemical study. *J Comp Neurol* **386**, 71–91.

Pombal MA, El Manira A & Grillner S (1997*b*). Organization of the lamprey striatum – transmitters and projections. *Brain Res* **766**, 249–254.

Pombal MA, Marin O & Gonzalez A (2001). Distribution of choline acetyltransferase-immunoreactive structures in the lamprey brain. *J Comp Neurol* **431**, 105–126.

Redgrave P, Gurney K, Reynolds J (2008). What is reinforced by phasic dopamine signals? *Brain Res Rev* **58**, 322–339.

Robertson B, Auclair F, Ménard A, Grillner S & Dubuc R (2007). GABA distribution in lamprey is phylogenetically conserved. *J Comp Neurol* **503**, 47–63.

Robertson B, Jones M, Samuelsson E, Hill R, Hellgren J & Grillner S (2009). The lamprey basal ganglia – a vertebrate blue-print. Meeting abstract, 566.10, Society for Neuroscience.

Robertson B, Stephenson-Jones MR, Ericsson J, Diaz Heijtz R & Grillner S (2010). The direct and indirect pathways of lamprey basal ganglia. Meeting abstract, 220.2, Federation of European Neuroscience Societies Forum.

Rogawski MA, Beinfeld MC, Hays SE, Hokfelt T & Skirboll LR (1985). Cholecystokinin and cultured spinal neurons. Immunohistochemistry, receptor binding, and neurophysiology. *Ann N Y Acad Sci* **448**, 403–412.

Rymar VV, Sasseville R, Luk KC & Sadikot AF (2004). Neurogenesis and stereological morphometry of calretinin-immunoreactive GABAergic interneurons of the neostriatum. *J Comp Neurol* **469**, 325–339.

Shen W, Hernandez-Lopez S, Tkatch T, Held JE & Surmeier DJ (2004). Kv1.2-containing K^+ channels regulate subthreshold excitability of striatal medium spiny neurons. *J Neurophysiol* **91**, 1337–1349.

Shen W, Tian X, Day M, Ulrich S, Tkatch T, Nathanson NM & Surmeier DJ (2007). Cholinergic modulation of Kir2 channels selectively elevates dendritic excitability in striatopallidal neurons. *Nat Neurosci* **10**, 1458–1466.

Standen NB & Stanfield PR (1978). A potential and time-dependent blockade of inward rectification in frog skeletal muscle fibres by barium and strontium ions. *J Physiol* **280**, 161–191.

Stephenson-Jones M, Samuelsson E, Ericsson J, Robertson B & Grillner S (2010). The core architecture of the basal ganglia – insights from evolution. Meeting abstract, P-64, International Basal Ganglia Society Meeting X.

Stern EA, Jaeger D & Wilson CJ (1998). Membrane potential synchrony of simultaneously recorded striatal spiny neurons in vivo. *Nature* **394**, 475–478.

Surmeier D, Ding J, Day M, Wang Z & Shen W (2007). D1 and D2 dopamine-receptor modulation of striatal glutamatergic signaling in striatal medium spiny neurons. *Trends Neurosci* **30**, 228–235.

Surmeier DJ, Stefani A, Foehring RC & Kitai ST (1991). Developmental regulation of a slowly-inactivating potassium conductance in rat neostriatal neurons. *Neurosci Lett* **122**, 41–46.

Tepper JM & Bolam JP (2004). Functional diversity and specificity of neostriatal interneurons. *Curr Opin Neurobiol* **14**, 685–692.

Tepper JM, Koos T & Wilson CJ (2004). GABAergic microcircuits in the neostriatum. *Trends Neurosci* **27**, 662–669.

Tepper J, Abercrombie E & Bolam J (2007). Basal ganglia macrocircuits. *Prog Brain Res* **160**, 3–7.

Thompson RH, Ménard A, Pombal M & Grillner S (2008). Forebrain dopamine depletion impairs motor behavior in lamprey. *Eur J Neurosci* **27**, 1452–1460.

Uchimura N, Cherubini E & North RA (1989). Inward rectification in rat nucleus accumbens neurons. *J Neurophysiol* **62**, 1280–1286.

Wallén P, Robertson B, Cangiano L, Low P, Bhattacharjee A, Kaczmarek LK & Grillner S (2007). Sodium-dependent potassium channels of a Slack-like subtype contribute to the slow afterhyperpolarization in lamprey spinal neurons. *J Physiol* **585**, 75–90.

Wilson C & Kawaguchi Y (1996). The origins of two-state spontaneous membrane potential fluctuations of neostriatal spiny neurons. *J Neurosci* **16**, 2397–2410.

Author contributions

J.E. conducted the experiments and primary data analysis and developed the experimental design together with M.W., G.S. and S.G.; B.R. provided expertise in neuroanatomical

methods; all authors took part in the evaluation of the experimental data. J.E. wrote the manuscript in interaction with all authors, who also approved the final version of the manuscript.

Acknowledgements

This work was supported by the Swedish Research Council, HEALTH-F2-2008-201716 select-and-act, ICT-STREP 216100-LAMPETRA, and the Karolinska Institute. We are grateful to Dr Peter Wallén for valuable comments on the manuscript.